Two-Dimensional Analysis of a Dust Explosion

Peak pressures and propagation velocities for dust explosions have for many years been studied as a function of particle concentration. There are, however, no multidimensional models in the literature which can be used to compute local pressures and impluses needed to access the potential damage caused by a detonation.

A two-dimensional two-phase hydrodynamic computer model was developed in this study to predict pressure propagation in dust explosions. Two cases of detonation of dispersed powders injected into a rectangular cavity were analyzed. The ignition of an idealized, uniformly distributed powder in a box produced a pressure peak that propagated through the powder with an increasing amplitude from the ignition source at one corner. The computational maximum pressure agreed with an approximate calculation of the Chapman-Jouguet pressure. The pressure propagation for the more realistic nonuniform initial particle distribution produced several peaks not unlike those observed on the ground below the detonation. Computed pressures agreed roughly with the measured average pressure peaks.

David F. Aldis
Dimitri Gidaspow
Department of Chemical Engineering
Illinois Institute of Technology
Chicago, IL 60616

Introduction

Every year people are killed and equipment is destroyed by dust explosions. The present death rate from grain dust explosions alone averages between five and fifteen people a year. During 1977 and 1978, the destruction caused by grain dust explosions amounted to over 100 million dollars. In 1986, several people died in a coal dust explosion in Japan. The potential explosion hazard extends to almost every industry that handles combustible bulk powders. Some of the powders that have been tested for explosibility by the U. S. Bureau of Mines are grain dusts, plastic dusts, metal dusts, and a large group of mixed dusts (Aldis and Lai, 1979). In Germany, the Berufsgenossenschaftliches Institut fur Arbeitssicherheit has reported test results for 809 powders (Field, 1982).

The phenomenon referred to in the popular press as a dust explosion is either a deflagration or a detonation. A deflagration is an exothermic process in which the gas pressure is relatively uniform with respect to space. A detonation is a process in which the pressure difference between the reactants and the combustion products is so large that a shock wave forms at the interface. The shock moves into the reactants at a speed that is equal to the sum of the material velocity of the products and the speed of sound of the combustion products. The reactants are heated by the shock, which then causes the reactants to deflagrate very quickly. This deflagration releases heat and moles of gas, causing a high pressure which, in turn, supports the shock. This concept of a detonation is called the ZND detonation theory, after the three researchers, Zeldovich, von Neumann, and Doring, who independently developed the analytical representation of the detonation process (Williams, 1985).

A detonation in an industrial setting is a devastating occurrence. It is possible to reduce the effects of a deflagration by venting the gas pressure formed by the combustion process. Since a deflagration is approximately a constant-pressure process, the vent keeps the gas pressure from increasing above the design limits of the building or the container holding the combusting reactants. However, if a detonation occurs, and if the vent is behind the detonation front, then the detonation will proceed ahead, and its progress will continue uninterrupted. Since the detonation is traveling at a speed that is greater than the speed of sound of the combustion products, the rarefaction front caused by the vent can never catch up with the detonation.

The present address of D. F. Aldis is Lawrence Livermore National Laboratory L-367, Livermore, CA 94550.

Literature Review

Dust explosions have been reported for over 200 years and have been studied for nearly as long. The history of dust explosions has been reviewed by several researchers (Palmer, 1974; Aldis and Lai, 1979; Field, 1982). This review is, therefore, restricted to only those works directly applicable to the present study.

The papers described below present experimental laboratory-scale dust explosion data and include some theoretical analysis. The work Butler et al. (1982) is concerned with the transition of a shock in a reactive propellant bed to a detonation. A paper by Gidaspow et al. (1986) presents data on the semifree field initiation of a suspended pyrotechnic material. The paper by Tamanini (1983) describes a research program on the deflagration of grain dust in a large combustion chamber. The paper by Gidaspow et al. (1984a) illustrates the numerical technique used in this paper.

Three lab-scale test programs have examined three different materials. Ogle (1986) studied aluminum dust deflagrations in a 20 L spherical chamber. His work is the best combined experimental and theoretical research program in the dust explosion area. Ogle's approach is based on principles of chemical kinetics and what he terms transport-driven fluid mechanics methodologies. Using existing literature on the combustion of aluminum, he was able to develop a viable reaction rate model that could then be used to describe his experimental results.

The Bureau of Mines report by Hertzberg et al. (1979) examined several experimental features of coal dust explosion testing. The report had little theoretical analysis, but it did present an excellent experimental research program. The program examined the effect of ignition energy on the minimum concentration necessary for an explosion. Subsequently, it was reported by Bartknect (1980) that it was necessary to use a chemical igniter which released at least 10 kJ to obtain results that scaled. Hertzberg examined the effect of the dust particle size on the rate of pressure rise in the combustion chamber. This rate is one of the most critical terms measured in a dust explosion test, and is used to determine the hazard class of the material. Hertzberg reports measurements of the temperature of both the dust particles and the gas surrounding the particles. The chamber used by Hertzberg was an 8 L cylinder with curved ends. The chamber had a length-to-diameter ratio of approximately one. A serious effort was made to verify the dust concentration in the vessel prior to ignition. The investigators used a light attenuation system calibrated with a material of known particle size and dispersal characteristics.

Grain dust was studied by Garrett (1981) and Lai et al. (1982). The explosion chamber used by Garrett was the Hartmann bomb. The Hartmann bomb has been reviewed by the American Society for Testing Methods (ASTM) as a standard device for studying dust explosions. It has, however, been reported by Bartknecht (1980) that the Hartmann bomb tends to underestimate the maximum rate of pressure rise as determined by vessels of different sizes. When vessels of different sizes are used, it is necessary to use the cube root scaling law to relate the results. When the results obtained with the Hartmann bomb are scaled and compared to the results obtained with, for example, spherical chambers of 20 L and 1 m^3 size, poor agreement is found. The reason given to explain this result is increased radiative heat loss in the Hartmann bomb. It has a minimum dimension of 4 in. compared to approximately 12 in. in the 20 L spherical chamber. Garrett reports the effects of dust chemical composition, particle size, and vessel shape and size. His work was well founded on both a firm semitheoretical chemical engineering analysis and a firm statistical basis.

An area that has not been exploited for use in dust explosion analysis research is the Department of Defense research in propellant shock-to-detonation transition (SDT) studies. One of the principal research groups that has emphasized this type of analysis is directed by Krier at the University of Illinois. His reports have developed a firm theoretical basis in this area. Applicable to the subject of this paper is his simulation of the shock transition of highly reactive propellants. For example, in a paper by Butler et al. (1982) results were reported for a simulation of the complete transition of a shock to a detonation.

In the paper by Gidaspow et al. (1986), the results of the initiation of a semiconfined dispersion of particulate reactive material were presented. The paper presented an analysis of the expected concentration distribution, showing that the particular method of dispersion seemed to give a relatively uniform distribution when the powder was properly injected, using several disseminators. However, when the dispersion was initiated, large pressure variations were observed on the ground as a function of time. Average pressures correlated well with Chapman-Jouguet pressures at various powder concentrations.

Tamanini (1983) reported a test program that examined large-scale deflagration of corn starch in a 2.4 × 2.4 × 12 m chamber. It is one of the largest chambers that has been used for a grain dust explosion study. In this vessel, a closed-to-open orientation was used in an attempt to obtain the most severe results possible.

Several flame speed models have been developed for the analysis of steady combustion (Glassmann, 1977). The models deal with either premixed or nonmixed gaseous combustion problems, usually at or near constant pressure. One of the models described by Glassmann was a one-dimensional, steady-state description of a laminar flame. In the model, it is assumed that conduction is the primary mechanism for the energy transfer. This model predicts that the flame speed is proportional to the square root of the combustion reaction rate, which has been experimentally verified. An extension of this theory to include radiation effects only becomes necessary when species that can absorb and reradiate the energy are present.

One series of theoretical studies on the deflagration of dust clouds was presented by Mitsui and Tanaka (1973) and Tanaka (1983). In these works, it is assumed that the principal mechanism for energy propagation in the gas phase is conduction through the gas between the combusting dust particles. This is a straightforward extension of the laminar flame theory described earlier. The effects of both convective gas heating of particles and of particle-to-particle radiation are included in this model. The cube root scaling relationship that has been observed experimentally was thereby explained.

Many industrial dust explosion hazards exist in tunnels, conveyors, and other large chambers having large length to diameter ratios. The chamber used by Tamanini (1983) is a good example of a typical industrial facility. It has a length-to-diameter ratio of about five. When a dust explosion occurs in a vessel of this type, the ignition phenomenon is a multidimen-

sional process. In this paper, a two-dimensional simulation of an ignition of a dispersed pyrotechnic particulate is described.

Theoretical Model

The reactive multiple-phase hydrodynamic model is based on the principles of mass, momentum, and energy conservation for each phase (Gidaspow, 1986). The contribution of the change in momentum of the combustion products has been added to the momentum equation, as done by Baer et al. (1986), to insure frame invariance. The partial differential equations that have been developed that use these principles are Eqs. 1 through 8.

Mass continuity equations

In Eqs. 1 and 2, the mass continuity equations are given for the gas phase and for the solid phase.

Gas Phase

$$\frac{\partial}{\partial t}(\epsilon\rho_g) + \frac{\partial}{\partial x}(\epsilon\rho_g U_g) + \frac{\partial}{\partial y}(\epsilon\rho_g V_g) = \dot{m}_s \tag{1}$$

Solid Phase

$$\frac{\partial}{\partial t}(\epsilon_s\rho_s) + \frac{\partial}{\partial x}(\epsilon_s\rho_s U_s) + \frac{\partial}{\partial y}(\epsilon_s\rho_s V_s) = -\dot{m}_s \tag{2}$$

Momentum equations

The momentum equations for the horizontal and vertical components, for both the gas and the solid phase are Eqs. 3, 4, 5, and 6.

Gas Momentum in x Direction

$$\frac{\partial}{\partial t}(\epsilon\rho_g U_g) + \frac{\partial}{\partial x}(\epsilon\rho_g U_g U_g) + \frac{\partial}{\partial y}(\epsilon\rho_g V_g U_g) = -\epsilon\frac{\partial P}{\partial x} - \left(\frac{\dot{m}_s}{2} + \beta_x\right)(U_g - U_s) \tag{3}$$

Momentum in x Direction for Solid Phase

$$\frac{\partial}{\partial t}(\epsilon_s\rho_s U_s) + \frac{\partial}{\partial x}(\epsilon_s\rho_s U_s U_s) + \frac{\partial}{\partial y}(\epsilon_s\rho_s V_s U_s) = -\epsilon_s\frac{\partial P}{\partial x} - \frac{\partial \tau}{\partial x} + \left(\frac{\dot{m}_s}{2} + \beta_x\right)(U_g - U_s) \tag{4}$$

Gas Momentum in y Direction

$$\frac{\partial}{\partial t}(\epsilon\rho_g V_g) + \frac{\partial}{\partial x}(\epsilon\rho_g U_g V_g) + \frac{\partial}{\partial y}(\epsilon\rho_g V_g V_g) = -\epsilon\frac{\partial P}{\partial x} - \left(\frac{\dot{m}_s}{2} + \beta_y\right)(V_g - V_s) \tag{5}$$

Momentum in y Direction for Solid Phase

$$\frac{\partial}{\partial t}(\epsilon_s\rho_s V_s) + \frac{\partial}{\partial x}(\epsilon_s\rho_s U_s V_s) + \frac{\partial}{\partial y}(\epsilon_s\rho_s V_s V_s) = -\epsilon_s\frac{\partial P}{\partial y} - \frac{\partial \tau}{\partial y} + \left(\frac{\dot{m}_s}{2} + \beta_y\right)(U_g - U_s) \tag{6}$$

Energy equations

The energy equations for the gas and the solid phases are Eqs. 7 and 8.

Gas Phase Conservation of Energy

$$\frac{\partial}{\partial t}(\epsilon\rho_g I_g) + \frac{\partial}{\partial x}(\epsilon\rho_g I_g U_g) + \frac{\partial}{\partial y}(\epsilon\rho_g I_g V_g) = -P\left[\frac{\partial \epsilon}{\partial t} + \frac{\partial}{\partial x}(\epsilon U_g) + \frac{\partial}{\partial y}(\epsilon V_g)\right] + h_{vs}(T_s - T_g) + \frac{\partial}{\partial x}\left(K_g\epsilon\frac{\partial t_g}{\partial x}\right) + \frac{\partial}{\partial y}\left(K_g\epsilon\frac{\partial T_g}{\partial y}\right) + \dot{m}_s\Delta E_i \tag{7}$$

Conservation of Energy of Solid Phase

$$\frac{\partial}{\partial t}(\epsilon_s\rho_s I_s) + \frac{\partial}{\partial x}(\epsilon_s\rho_s I_s U_s) + \frac{\partial}{\partial y}(\epsilon_s\rho_s I_s V_s) = P\left[\frac{\partial \epsilon_s}{\partial t} + \frac{\partial}{\partial x}(\epsilon_s U_s) + \frac{\partial}{\partial y}(\epsilon_s V_s)\right] + h_{vs}(T_g - T_s) + \frac{\partial}{\partial x}\left(K_s\epsilon_s\frac{\partial T_s}{\partial x}\right) + \frac{\partial}{\partial y}\left(K_s\epsilon_s\frac{\partial T_s}{\partial y}\right) \tag{8}$$

Separate mass continuity, momentum, and energy equations are used for both the gas (continuous) phase and the solid phase. The variables predicted are the void fraction, the gas pressure, the temperatures of the gas and solid phases, the vertical velocity components of the gas and solid phases, and the horizontal velocity components of the gas and solid phases. The effect of the variation of particle size was also studied by including the particle size as an additional independent variable (Aldis, 1987). The effect was found to be small.

Constitutive equations

In this section the constitutive equations are explicitly defined. The constants in these equations are defined later for each specific problem.

In a multiple-phase system, one of the most important coefficients is the fluid particle drag. The form for the fluid particle drag used throughout paper is that previously used by Gidaspow et al. (1986). The equations used to calculate the drag coefficients are Eqs. 9 and 10.

$$\beta_x = \beta_y = \frac{150\epsilon_s^2\mu}{\epsilon(d_s\phi_s)^2} + \frac{1.75\rho_g|V_g - V_s|\epsilon_s}{(d_s\phi_s)} \quad \text{for} \quad 0.2 \le \epsilon < 0.8 \tag{9}$$

and

$$\beta_x = \beta_y = \frac{3}{4}\frac{C_{Ds}\epsilon|V_g - V_s|\rho_g\epsilon_s f(\epsilon)}{(d_s\phi_s)} \quad \text{for} \quad 0.8 \le \epsilon \le 1.0 \tag{10}$$

where

$$f(\epsilon) = \epsilon^{-2.65}$$

$$C_{Ds} = \frac{24}{Re_s}(1 + 0.15Re_s^{0.687}), \quad \text{for} \quad Re_s < 1{,}000$$

Table 1. Density in Bag at Time of Initiation, kg/m³

Vertical Height m	Horizontal Position, m									
	0.2	0.4	0.6	0.8	1.0	1.2	1.4	1.6	1.8	2.0
0.06	21.77	7.31	6.72	6.70	6.98	7.48	8.17	9.36	11.89	33.33
0.12	11.77	0.39	0.15	0.16	0.18	0.22	0.28	0.41	0.76	14.21
0.18	8.42	0.07	—	—	—	—	—	0.02	0.06	11.99
0.24	6.53	0.02	—	—	—	—	—	—	0.03	11.89
0.30	6.04	—	—	—	—	—	—	—	0.06	12.39
0.36	3.88	1.93	1.08	0.72	0.53	0.42	0.34	0.31	0.30	14.17
0.42	2.39	3.29	2.70	2.08	1.62	1.29	1.07	0.92	0.85	19.41
0.48	1.96	5.29	7.74	9.19	10.13	10.78	11.25	11.63	12.28	50.62
0.54	2.66	3.73	3.17	2.54	2.08	1.78	1.60	1.51	1.54	20.54
0.60	4.73	2.33	1.34	0.96	0.75	0.64	0.56	0.53	0.53	14.65
0.66	8.05	—	—	—	—	—	—	0.02	0.12	12.59
0.72	8.72	—	—	—	—	—	—	—	0.06	12.02
0.78	11.15	0.03	—	—	—	—	—	0.02	0.07	12.10
0.84	15.44	0.17	0.12	0.13	0.16	0.20	0.26	0.38	0.72	14.23
0.90	29.69	8.86	7.69	7.47	7.62	8.00	8.57	9.66	12.12	33.59

and

$$C_{Ds} = 0.44, \quad \text{for} \quad Re_s \geq 1{,}000$$

The development of the set of equations describing particle gas hydrodynamics has been reviewed by many researchers, including Gidaspow (1986). It has proven necessary to include a term that prevents the solid from becoming infinitely compressed. Rietma and Mutsers (1979) introduced a term into a fluidization model to account for this effect. This solid stress term, as described by Gidaspow (1986), is a function of the void fraction as shown in Eq. 11.

$$\tau = \tau(\epsilon) \tag{11}$$

By chain rule Eq. 11 is expanded as follows:

$$\frac{\partial \tau}{\partial y} = \frac{\partial \tau}{\partial \epsilon}\frac{\partial \epsilon}{\partial y} \tag{12}$$

The solids stress coefficient is defined in Eq. 13.

$$G(\epsilon) = \frac{\partial \tau}{\partial \epsilon} \tag{13}$$

Table 2. Initial Conditions for Two Dispersed Pyrotechnic Problems

Variable	Uniform Density Problem	Nonuniform Density Problem
Initial Gas Temp., K	298.0	298.0
Initial Particle Temp., K	298.0	298.0
Initial Press., bar	1.0	1.0
Particulate Conc., kg/m³	5.0	Table 1
Ignitor Temp., K	4,000.0	4,000.0
Ignitor Press., GPa	1.0	1.0
Ignitor size, cells	1.0	2.0

The solids stress coefficient used in this paper is given in Eq. 14.

$$-G(\epsilon) = e^{a(1-\epsilon)} \tag{14}$$

This form of the solids stress uses a power of e rather than 10 so that the double-precision exponential function can be used in the computational solution directly.

The fluid particle heat transfer coefficient used in this paper is that used by Butler et al. (1982) and is given in Eq. 15.

$$h = 0.65\left(\frac{K_g}{d}\right) Re^{0.7} Pr^{0.33} \tag{15}$$

The thermal conductivity of the gas is expressed with respect to a reference temperature T_{g0}:

$$K_g = K_0\left(\frac{T_g}{T_{g0}}\right)^{1.786} \tag{16}$$

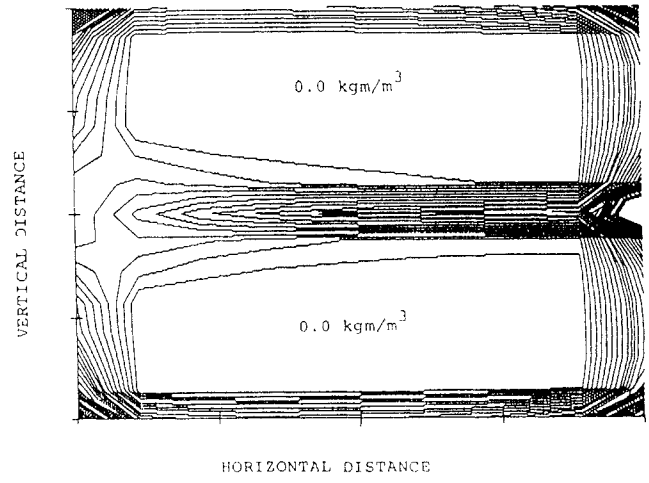

Figure 1. Contour plot of nonuniform density field.
Contour lines at 1 kg/m³ increments

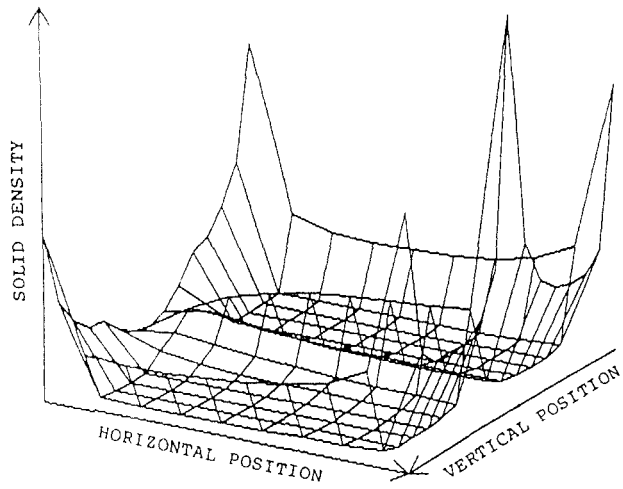

Figure 2. Three-dimensional surface plot of initial nonuniform density distribution.

The thermal conductivity of the dispersed particulate has been assumed to be zero for the problems studied in this paper. It is assumed that the detonation-like processes being studied have material velocity magnitudes much greater than any anticipated thermal wave velocity that might be transmitted through the dispersed particulate.

The constant-volume heat capacity of the gas was assumed constant at 1.773 kJ/kg · K. The specific heat of the solid particulate was assumed to be independent of particle size and constant at 1.266 kJ/kg · K.

The gas was assumed to be nonideal and its equation of state is given by:

$$\frac{PV}{nR_gT} = 1.0 + 2.5\rho_g - 0.5\rho_g^2 \tag{17}$$

The molecular weight of the gas was assumed to be 26 g/mol.

The solid decomposition rate, $\dot{m}_s$, used in this paper is given a power law form with respect to pressure, as used by Butler et al. (1982), and is given in Eq. 18.

$$\dot{m}_s = \frac{3a\rho_s\epsilon_s}{R} P^b \tag{18}$$

where

$$R = R_0\left(\frac{\rho_s\epsilon_s}{\rho_s\epsilon_{s,0}}\right)^{1/3} \tag{19}$$

Solution procedure

The solution procedure used to solve the set of partial differential equations, Eqs. 1–8, is similar to that used by Syamlal (1985, 1987) and by Rivard and Torrey (1976), with some differences. The two energy equations are solved using a matrix method called the LU decomposition technique, as described by Stark (1970). This matrix solution procedure is used in both the implicit and explicit steps of the solution process. Because the matrix procedure is exactly the same, it is contained in a separate subroutine that is called for in both the implicit and the explicit steps. The computer program was presented by Aldis (1987).

Experimental studies of pyrotechnic dust explosions

Gidaspow et al. (1984b, 1986) and Austing et al. (1986) have measured the gas overpressure created by a semiconfined dispersed particulate detonation of TNT. The cloud was formed in a box 0.88 × 4.0 × 0.88 m by injecting particles into the rectangular cavity by means of one or more disseminators. One of the long sides of the box was on the ground. The remaining sides were made of 0.152 mm polyethylene film, covered by 0.25 in hardware cloth (metal) screen. Overpressures were measured by piezoelectric transducers (gauges) mounted in steel plates on the ground. An ignitor was located just above the ground at the left end of the box. The igniter was 100 g of composition C-4 high explosive.

Modeling of pyrotechnic dust explosions and concentrations

Gidaspow et al. (1984b, 1986) used the multiple-phase hydrodynamic computer program MULTIFIX to predict the particulate densities in the experimental dispersion system described above. The predictions were transient contours of the two-dimensional density field. The motion of the front was measured with high-speed motion pictures. The measured motion agreed with the computations. In Table 1, one of the early density fields predicted by Gidaspow et al. (1986) is shown as a function of vertical position and distance from the end of the box containing the cloud.

Previous modeling efforts on the detonation of dispersed materials have been reported by Lee and Sichel (1985) and Wolanski et al. (1983). The most advanced of these models, that by Lee and Sichel, was a steady-state, one-dimensional calculation. The coordinate system was established so the origin of the spatial variable followed the detonation front. The dispersed particulate was assumed to be stationary with respect to a fixed coordinate system as the shock entered the dispersed particulate. The velocity of the shock front going into the dispersed

Table 3. Parameter Values for Two Dispersed Pyrotechnic Problems

Variable	Uniform Density Problem	Nonuniform Density Problem
Theoret. max. Particle density, g/cm^3	2.0	2.0
Gaseous molec. wt.	26.0	26.0
Particle size, d_1 μm	30.0	30.0
Gaseous const. vol. specific heat, J/g · K	1.773	1.773
Particle const. vol. specific heat, J/g · K	1.2665	1.2665
Chem. reac. energy released, kJ/g	5.48	5.48
Surface regress. const., cm/s (Pa)	2.21×10^{-6}	2.21×10^{-6}
Pressure exponent, b	1.0	1.0
Chamber ht., in	0.88	0.88
Chamber length, m	2.0	2.0
No. Horizontal cells	82.0	82.0
No. Vertical Cells	37.0	37.0

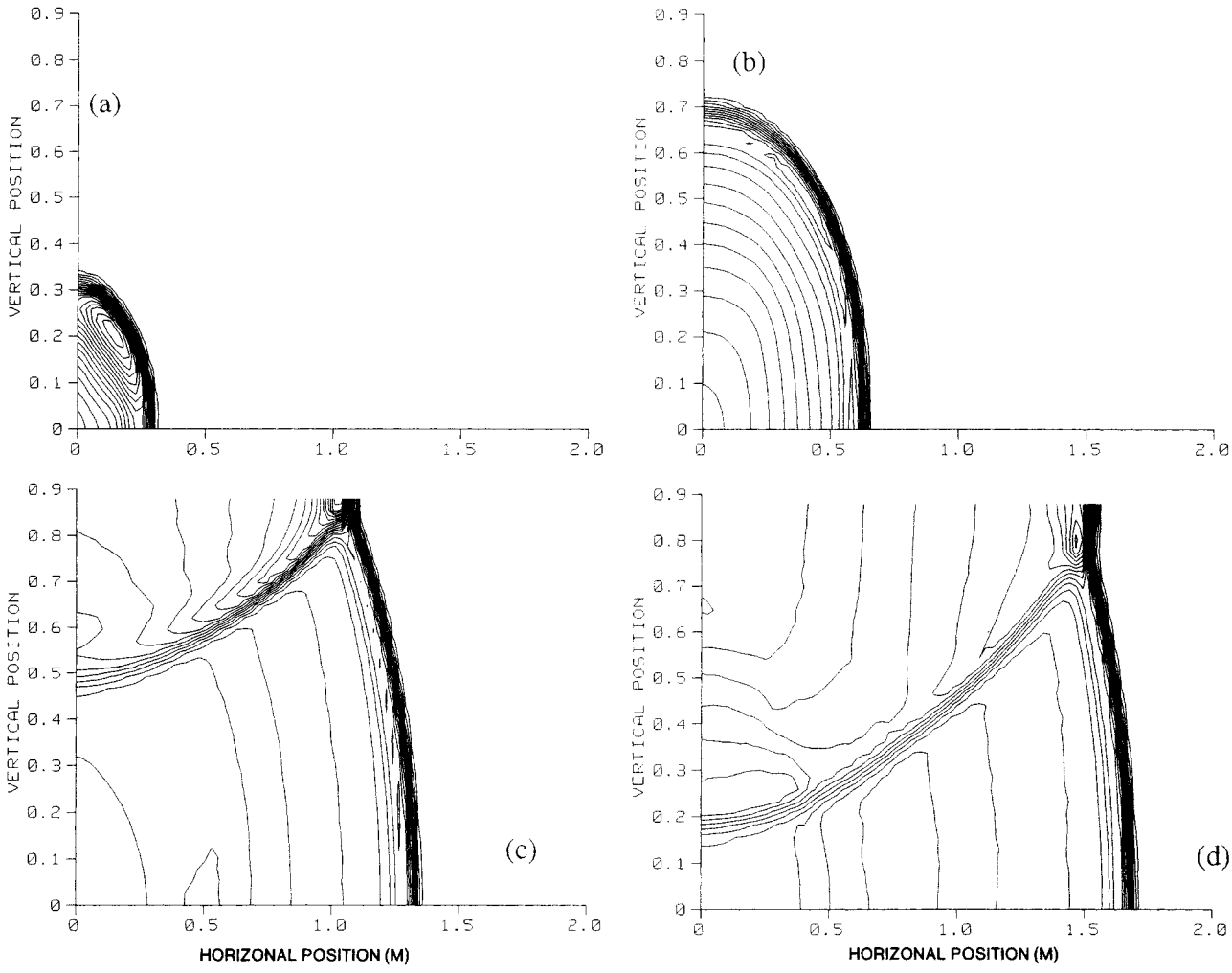

Figure 3. Contour plots of pressure field, uniform density problem.

Contour lines at 10 bar increments (a) at 0.1 ms; (b) at 0.4 ms; (c) at 0.7 ms; (d) at 0.9 ms

particulate was adjusted to obtain a Chapman-Jouguet state at the right boundary of the computational grid, just as the particulate was completely consumed.

Description of the Physical System Modeled

In this paper, the detonation of a dispersion of particulates is simulated by numerically solving Eqs. 1–8. A two-dimensional rectangular coordinate system is used. The system being modeled is similar in size and shape to that simulated by Gidaspow et al. (1984b) for dispersion of powders.

The confining walls were assumed to be firm. It was assumed that they would not yield in the first millisecond after the igniter was detonated. The validity of this assumption is shown later.

Initial and boundary conditions

Two solutions are presented in this paper for this dispersed particulate problem. The initial conditions for both of the problems are given in Tables 1 and 2. In Table 2, the initial conditions for the first simulation include a uniform particulate concentration of 5.0 kg/m^3. The particulate concentration for the second simulation is that predicted by Gidaspow et al. (1984b). The particulate concentration is given in Table 1 as a function of vertical height and distance from the left wall of the box. The same data are shown graphically in Figures 1 and 2. Figure 1 is a contour plot of the density field. In this plot, lines are drawn through points at which values of density are

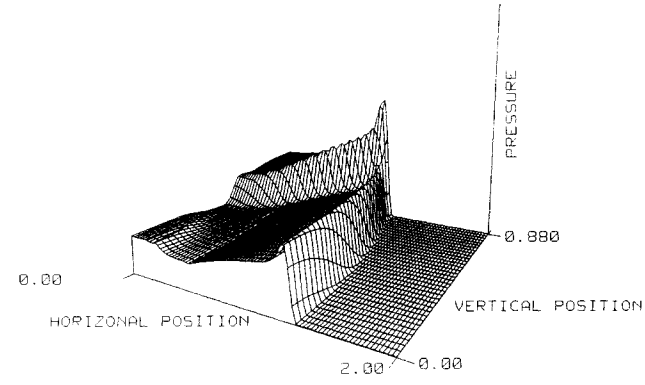

Figure 4. Three-dimensional surface plot of pressure field, uniform density problem.

At 0.7 ms; max. pressure 258 bar

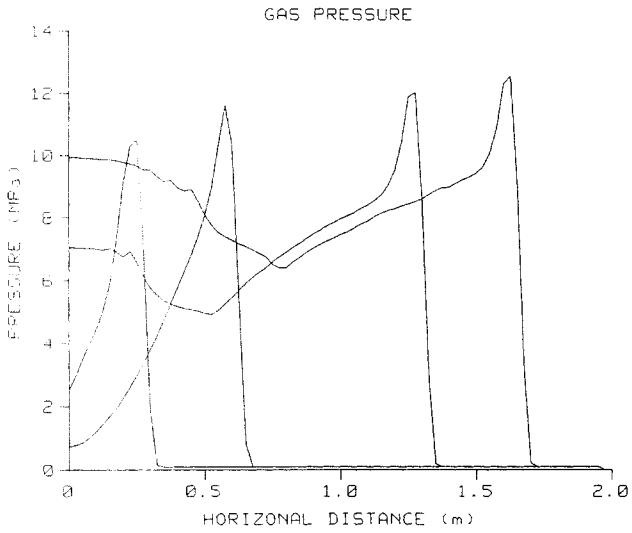

Figure 5. Pressure on ground during uniform density calculation.
At 0.1, 0.4, 0.7, 0.9 ms

constant. The lowest density is zero and the highest is approximately 50 kg/m^3. The contour lines are drawn at increments of 1.0 kg/m^3. In Figure 2, the data are presented in a three-dimensional surface plot. In this graph, the perpendicular distance from the base plane is proportional to the density. In all of these representations, the density field is shown to be nonuniform. There are high-density regions on the top and bottom surfaces and in the center of the container. The average density of the field is approximately 4.7 kg/m^3.

Additional parameters for both of the dispersed pyrotechnic material problems are given in Table 3. The problems were kept very similar so that the effect of the nonuniform concentration could be isolated.

The high explosive igniter, located at the bottom left corner of the box, is approximated as a 2.5 × 5.0 cm rectangular box of gas at a pressure of 1.0 GPa and a temperature of 4,000 K. As described later, this igniter size appears to be adequate to cause all of the particulate to be consumed.

Computational results

The most significant result from the two-dimensional, dispersed reactive multiple-phase hydrodynamic analysis is the

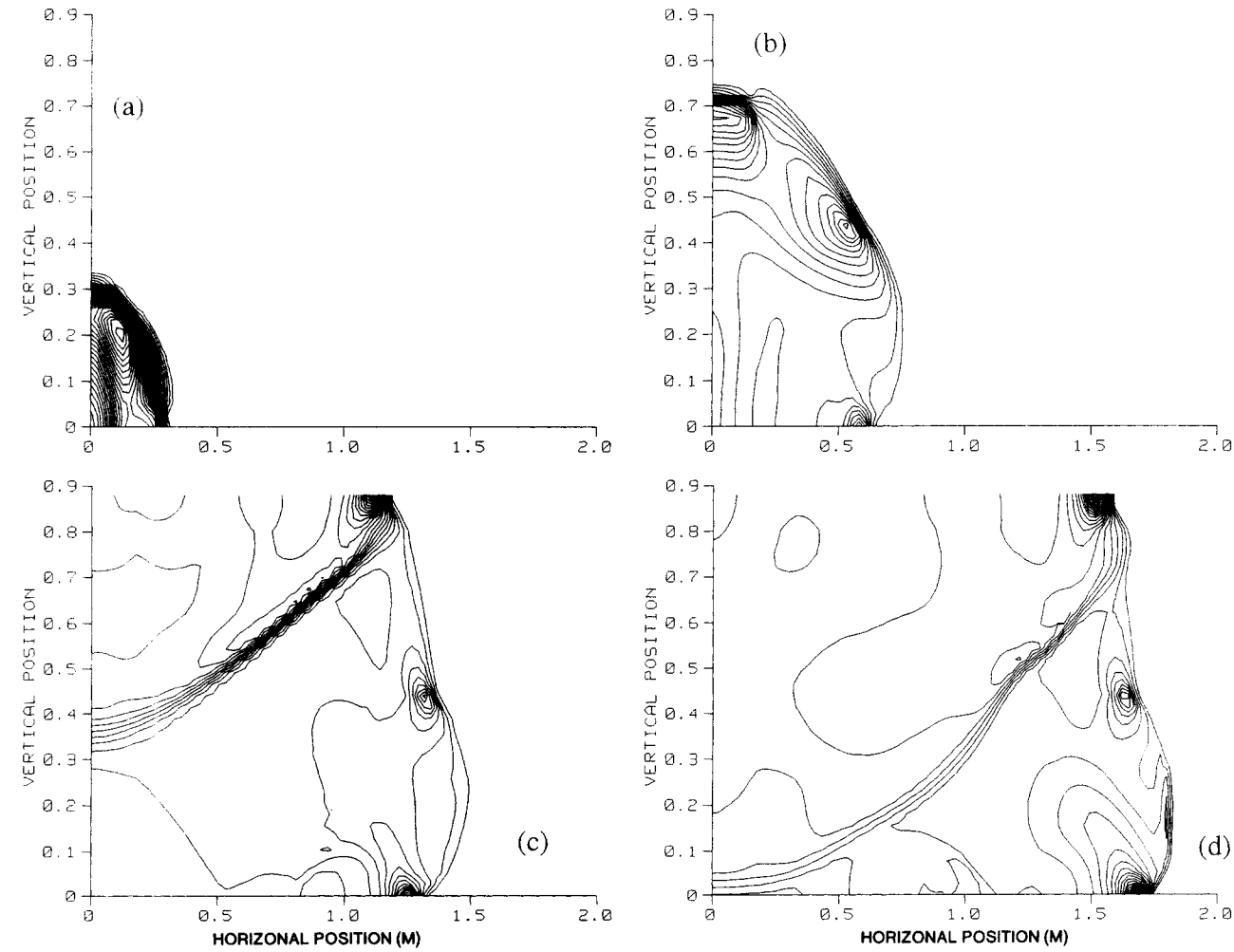

Figure 6. Contour plots of pressure field, nonuniform density problem.
Contour lines at 10 bar increments (a) at 0.1 ms; (b) at 0.4 ms; (c) at 0.7 ms; (d) at 0.9 ms

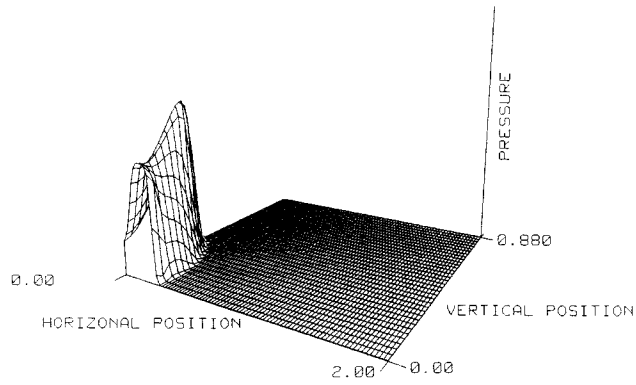

Figure 7. Three-dimensional surface plot of pressure field, nonuniform density problem.
At 0.1 ms; max. pressure 287 bar

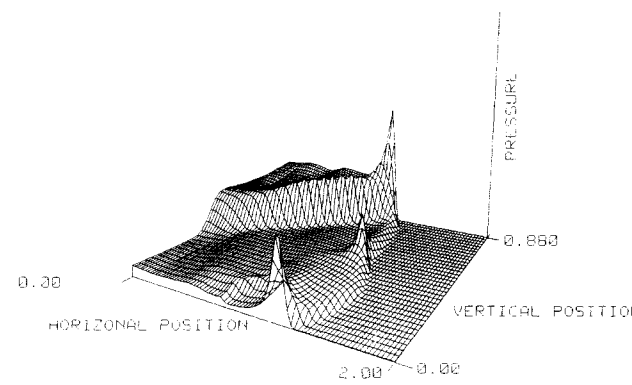

Figure 9. Three-dimensional surface plot of pressure field, nonuniform density problem.
At 0.7 ms; max. pressure 252 bar

transient pressure field. Two aspects of this field are of direct relevance, the peak pressure and the propagation velocity. Both of these variables can be estimated independently, theoretical by assuming that a Chapman-Jouguet (CJ) state is present just behind the reaction front. To use this estimate, however, one must assume that the flow is one-dimensional, which is not the case for the problem studied in this section.

One method of displaying computational results from a two-dimensional calculation is by using a contour plot, as was done for the nonuniform density field. The pressure at 0.1, 0.4, 0.7, and 0.9 ms are shown in contour plots in Figures 3a, 3b, 3c, and 3d, respectively. The detonation front expands to the right and up, into the low-pressure region containing the particulate. This method of examining the computational results gives a good qualitative appreciation of the overall results without sorting though pages of numerical data.

A second method for displaying two-dimensional computational results is a three-dimensional surface plot, such as was also done for the nonuniform density field. Figure 4 shows an example for this calculation at a time of 0.7 ms. The three-dimensional surface plot gives a qualitative appreciation of the overall pressure field. Specific features of the flow can quickly be identified and evaluated.

A third way of presenting the predicted results is by looking specifically at the variable that corresponds most closely to that which was measured in the experiment being simulated. Therefore, in Figure 5 the pressure on the surface of the ground is presented as a function of distance from the left end of the box at times of 0.1, 0.4, 0.7, and 0.9 ms. If a pressure gauge were swept over by the pressure field, the signals from it would look very similar to those shown in Figure 5, except that the distance variable would be replaced by the negative of the time variable.

The maximum pressure that would be estimated from an idealized one-dimensional CJ calculation can be calculated using the equations below:

$$P_{cj} = 2\frac{(q + e_0)(\gamma - 1)}{V_0}$$

$$V_{cj} = 2(\gamma^2 - 1)(q + e_0) \tag{20}$$

Using these equations, the expected detonation pressure has been estimated at 109×10^5 Pa. The predicted value shown in Figure 5 is 126×10^5 Pa. The agreement is better than expected. This phenomenon is not an ideal detonation moving into a uniform density field, as described next.

The results for the nonuniform density field are shown at times of 0.1, 0.4, 0.7, and 0.9 ms in contour plots in Figures 6a, 6b, 6c, and 6d, respectively. Three-dimensional surface plots are shown in Figures 7–10. The development of the detonation-like

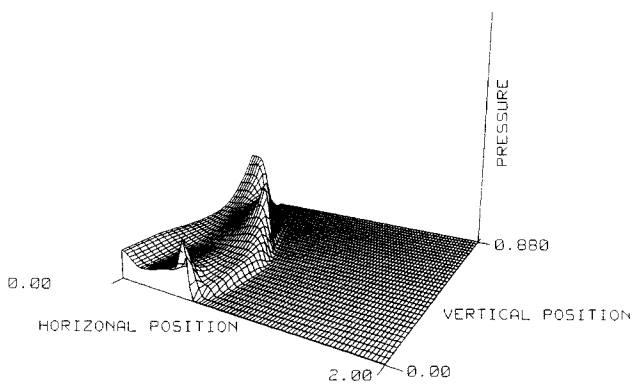

Figure 8. Three-dimensional surface plot of pressure field, nonuniform density problem.
At 0.4 ms; max. pressure 153 bar

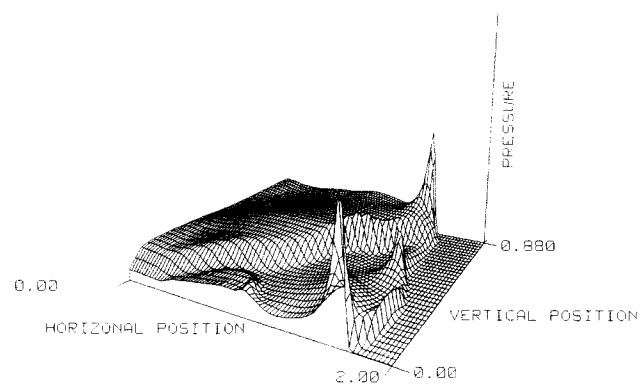

Figure 10. Three-dimensional surface plot of pressure field, nonuniform density problem.
At 0.9 ms; max. pressure 227 bar

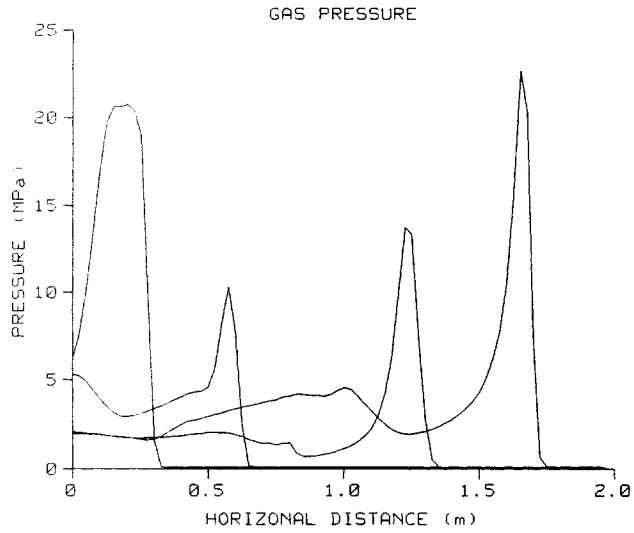

Figure 11. Pressure on ground during nonuniform density calculation.
At 0.1, 0.4, 0.7, 0.9 ms

process is substantially different for the reaction propagation into the nonuniform density field than for the propagation into the uniform field. After the first time period of 0.115 ms, the pressure contours have already begun to become noncylindrical. This nonsymmetric shape is easily seen in the three-dimensional surface plot in Figure 7.

When the reaction front moves toward the top wall, as shown in Figure 6b, it appears that the front at the original point of ignition in the lower left corner of the chamber has died out. But in Figure 8 a more correct picture can be seen. The reaction front is still propagating at the point of ignition, but the reflected reaction front coming off the top of the chamber is so strong that the original front is dwarfed in comparison.

The final results at 0.7 and 0.9 ms shown in contour plots in Figures 6c and 6d and in three-dimensional surface plots in Figures 9 and 10 show an interesting result. The uniform density calculation results, given in Figures 3c and 3d, show that the reaction front from the ignition point and the front which developed from the reflected shock from the top of the chamber seem to coalesce at 0.9 ms. In the case for the nonuniform density problem, three distinct reaction fronts become visible, separated by the regions of very low density. These reaction spikes cannot be approximated in any reasonable way as planar detonation field. Therefore, the interpretation of the spike pressures and wave velocities cannot be estimated using Chapman-Jouguet theory of planar detonations.

The predicted ground pressures are shown in Figure 11 at times of 0.1, 0.4, 0.7, and 0.9 ms. These values are likely to be good estimates of the results that were measured experimentally for the time period presented. However, in Figure 10 an expansion wave can be seen moving toward the ground plane. When this disturbance hits the ground, the pressure will rise dramatically. It has been assumed that the sides of the chamber are firm. This approximation allows one to make a good estimate of the ground pressure until the reflected shock from the top of the chamber can communicate with the ground. If the chamber walls are weak, then a rarefaction wave will propagate into the reacting flow in a manner similar to how the reflected wave moves toward the ground. The velocity of the reflected wave will be greater than that of a rarefaction front. The rarefaction wave velocity will be the speed of sound of the mixture, but reflection wave velocity will be the velocity of a shock. The shock always has to move faster than the speed of sound or the shock would dissipate. Therefore, the predicted pressures on the ground should be accurate for about 1.0 ms.

A comparison between the experimental results of Gidaspow et al. (1984b) and those of this paper is shown in Figure 12. The predicted results are well within the scatter of the experimental data.

The two-dimensional methods used in the paper can easily be extended to a three-dimensional version, but the added computational overhead does not seem at this time to be justified.

Acknowledgment

This research was performed with support of and in cooperation with IIT Research Institute, Chicago, Illinois. Without the earlier efforts of James Austing, Alan Tulis, and William Sumida this work would not have been possible. We acknowledge an anonymous reviewer of an

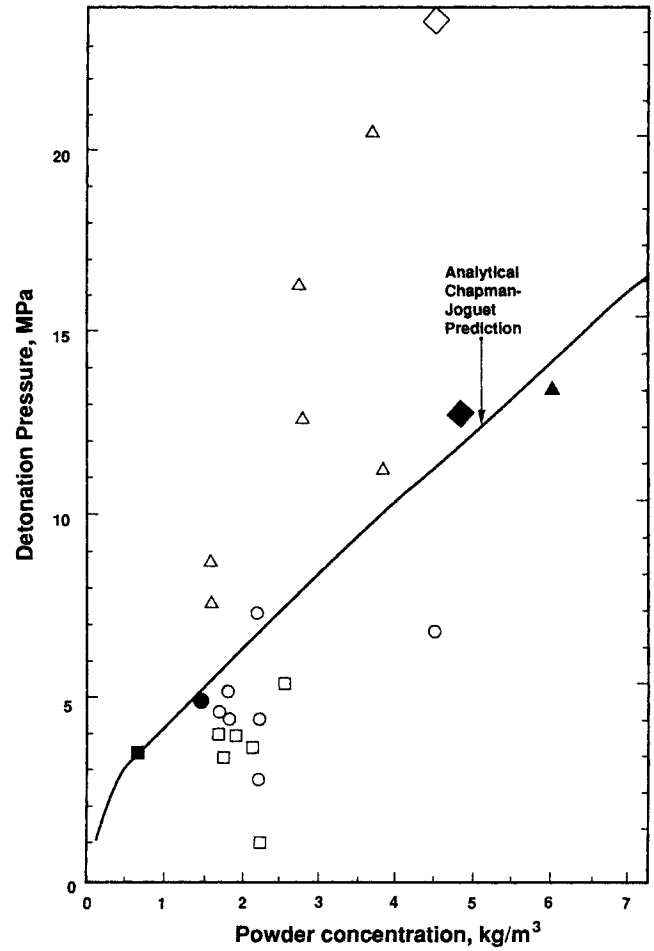

Figure 12. Comparison of calculated results (this paper) and experimental results (Gidaspow et al., 1984 b).
○ Test 12; □ Test 14; △ Test 16
Averaged values: ●■▲
Computational results: ◊ uniform density problem; ♦ nonuniform density problem.

earlier version of this paper for pointing out a formulation error. The assistance given by M. Syamlal was also extremely helpful.

Notation

a, b = constants
d = particle diameter
e_0 = energy at reference state
G = solids stress
h = particle, gas heat transfer coefficient
h_v = volumetric heat transfer coefficient between solid and gas
I_i = constant composition internal energy
K_g = gaseous thermal conductivity at T_g
K_0 = gaseous thermal conductivity at T_{g0}
K_s = solid thermal conductivity
$\dot{m}_s$ = solid combustion rate
n = number of moles
P = gas pressure
P_{cj} = Chapman-Jouguet pressure
Pr = Prandtl number
q = chemical energy released during detonation
R = particle radius
R_0 = initial particle radius
R_g = universal gas constant
Re = Reynolds number for particle in gas
t = time
T_g = gas temperature
T_s = solid temperature
U_i = horizonal velocity, $i = g$(gas), s(solid)
V = gas volume
V_0 = specific volume before detonation
V_{cj} = Chapman-Jouguet detonation velocity
V_i = vertical velocity, $i = g$(gas), s(solid)
x = horizontal coordinate
y = vertical coordinate

Greek letters

β_x = horizontal momentum transfer coefficient between solid and gas
β_y = vertical momentum transfer coefficient between solid and gas
ΔE_s = energy of reaction for solid decomposition
ϵ = gas volume fraction
ϵ_s = solid volume fraction
$\epsilon_{s,0}$ = initial solid volume fraction
γ = ratio of specific heats of product gases
ρ_g = gas density
ρ_s = solid density

Literature Cited

Aldis, D. F., "Reactive Multiple-phase Hydrodynamics," PhD Diss., Illinois Inst. Technol., Chicago (1987).

Aldis, D. F., and F. S. Lai, *Review of Literature Related to Engineering Aspects of Grain Dust Explosions,* U.S. Dept. Agriculture, Misc. Pub. No. 1375 (1979).

Austing, J. L., A. J. Tulis, W. K. Sumida, D. Gidaspow, "The Large-Scale Unconfined Detonation of Dispersed Fuels and Pyrotechnics in a Controlled Geometry Enclosure," 13th Symp. Explosives and Pyrotechnics, 193 (1986).

Baer, M. R., R. J. Gross, and J. W. Nunziato, "An Experimental and Theoretical Study of Deflagration-to-Detonation Transition (DDT) in the Granular Explosive CP," *Combust. Flame,* **65,** 15 (1986).

Bartknecht, W., *Explosions Course Prevention Protection,* Springer, Berlin (1980).

Butler, P. B., M. F. Lembeck, and H. Krier, "Modeling of Shock Development and Transition to Detonation Initiated by Burning in Porous Propellant Beds," *Combust. Flame,* **46,** 75 (1982).

Field, P., *Dust Explosions,* Elsevier, New York (1982).

Garrett, D. W., "Study of Mechanisms of Grain Dust Explosions as Affected by Particle Size and Composition," M.S. Thesis, Dept. Chem. Eng., Kansas State Univ., Manhattan, KS (1981).

Gidaspow, D., "Hydrodynamics of Fluidization and Heat Transfer: Supercomputer Modeling," *Appl. Mech. Rev.,* **39**(1), 1 (1986).

Gidaspow, D., B. J. Ettehadieh, and M. Syamlal, "Hydrodynamics of Fluidization: Bubbles and Gas Compositions in the U-gas Process," *Am. Inst. Chem. Eng. Meet.,* San Francisco (1984a).

Gidaspow, D., M. Syamlal, J. Austing, A. Tulis, K. Sumida, and W. Comeyne, "The Large-scale Detonation of a Particulate Pyrotechnic," *Int. Pyrotechnics Sem.* Colorado Springs, CO, 193 (Aug., 1984b).

Gidaspow, D., Y. Tsuo, A. Austing, and A. Tulis, "Simulation of Pyrotechnic Power Distributions Using a Hydrodynamic Multiparticle-size Computer Model," *11th Int. Pyrotechnics Sem.,* Vail, CO, 227 (July, 1986).

Glassman, I., *Combustion,* Academic Press, New York (1977).

Hertzberg, M., K. L. Cashdollar, and J. J. Opferman, *The Flamability of Coal Dust-Air Mixtures Lean Limits, Flame Temperatures, Ignition Energies, and Particle Size Effects,* Rept. of Invest. 8360, U.S. Dept. Interior, Bur. Mines, Washington, DC (1979).

Lai, F. S., D. W. Garrett, and L. T. Fan, "Study of Mechanisms of Grain Dust Explosions as Affected by Particle Size and Composition. I: Review of Literature," *Powder Technol.* **32,** 193 (1982).

Lee, D., and M. Sichel, "The Chapman-Jouguet Condition and Structure of Detonation in Dust-Oxidizer Mixtures," *Dynamics of Explosions,* Martin Summerfield, ed., Am. Inst. Aeronautics Astronautics, New York (1985).

Mitsui, R., and T. Tanaka, "Simple Models of Dust Explosion. Predicting Ignition Temperature and Minimum Explosive Limit in Terms of Particle Size," *Ind. Eng. Chem. Process Des. Dev.,* **12,** 384 (1973).

Ogle, R. A., "A New Strategy for Dust Explosion Research: A Synthesis of Combustion Theory, Experimental Design, and Particle Characterization," Ph.D. Thesis, Univ. Iowa, Iowa City (1986).

Palmer, K. N., *Dust Explosions and Fires,* Chapman and Hall, London (1974).

Rietma, K., and S. M. P. Mutsers, "The Effect of Interparticle Forces on Expansion of Homogeneous Gas-fluidized Bed," *Proc. Int. Symp. Fluidization,* Toulouse, 32 (1979).

Rivard, W. C., and M. D. Torrey, *KFIX: A Computer Program for Transient Two-dimensional Two-fluid Flow,* Rept No. LA-Nureg 6623, Los Alamos Nat. Lab., Univ. of California, Los Alamos, NM (1976).

Syamlal, M., "Mutiphase Hydrodynamics of Gas–Solid Flow," Ph.D. Diss. Illinois Inst. Technol., Chicago (1985).

———, *NIMPF: A Computer Code for Nonisothermal Multiparticle Fluidization,* Final Rept., Contract No. DE-AC21-85M C21353, EG & G, Washington Analyt. Serv. Center, Morgantown, WV (Feb., 1987).

Stark, P., *Introduction to Numerical Methods,* Macmillan, London, (1970).

Tamanini, F., *Dust-Explosion Propagation in Simulated Grain Conveyor Galleries,* Rept. No. ESV-83-067, Nat Grain Feed Assoc., Fire and Explosion Res. Rept., Washington, DC (1983).

Tanaka, T., "Theoretical Approaches to Dust Explosions," *Kona,* No. 1 (1983).

Williams, F. A., *Combustion theory,* Benjamin/Cummings, Menlo Park, CA (1985).

Wolanski, P., D. Lee, M. Sichel, C. Kauffman, and J. Nicholls. "The Structure of Dust Detonations," *9th Colloq. Dynamics of Explosions and Reactive Systems,* Poitiers, France (July, 1983).

Manuscript received Dec. 21, 1989, and revision received May 16, 1990.